Spectroelectrochemical Signatures of Surface Trap Passivation on CdTe Nanocrystals

Van Der Stam, Ward; Du Fossé, Indy; Grimaldi, Gianluca; Monchen, Julius O.V.; Kirkwood, Nicholas; Houtepen, Arjan J.

DOI
10.1021/acs.chemmater.8b03893

Publication date
2018

Document Version
Final published version

Published in
Chemistry of Materials

CHEMISTRY OF MATERIALS
Cite This: Chem. Mater. 2018, 30, 8052−8061
Article
pubs.acs.org/cm

Spectroelectrochemical Signatures of Surface Trap Passivation on CdTe Nanocrystals

Ward van der Stam,*[,§] Indy du Fossé,[§] Gianluca Grimaldi, Julius O. V. Monchen, Nicholas Kirkwood, and Arjan J. Houtepen*

Optoelectronic Materials Section, Faculty of Applied Sciences, Delft University of Technology, van der Maasweg 9, 2629 HZ Delft, The Netherlands

Supporting Information

ABSTRACT: The photoluminescence (PL) quantum yield of semiconductor nanocrystals (NCs) is hampered by in-gap trap states due to dangling orbitals on the surface of the nanocrystals. While crucial for the rational design of nanocrystals, the understanding of the exact origin of trap states remains limited. Here, we treat CdTe nanocrystal films with different metal chloride salts and we study the effect on their optical properties with *in situ* spectroelectrochemistry, recording both changes in absorption and photoluminescence. For untreated CdTe NC films we observe a strong increase in the PL intensity as the Fermi-level is raised electrochemically and trap states in the bandgap become occupied with electrons. Upon passivation of these in-gap states we observe an increase in the steady state PL and, for the best treatments, we observe that the PL no longer depends on the position of the Fermi level in the band gap, demonstrating the effective removal of trap states. The most effective treatment is obtained for Z-type passivation with $CdCl_2$, for which the steady state PL increased by a factor 40 and the PL intensity became nearly unaffected by the applied potential. X-ray Photoelectron Spectroscopy measurements show that treatment with $ZnCl_2$ mainly leads to X-type passivation with chloride ions, which increased the PL intensity by a factor four and made the PL less susceptible to modulation by applying a potential with respect to unpassivated nanocrystal films. We elucidate the spectroelectrochemical signatures of trap states within the bandgap and conclude that undercoordinated Te at the surface constitutes the largest contribution to in-gap trap states, but that other surface states that likely originate on Cd atoms should also be considered.

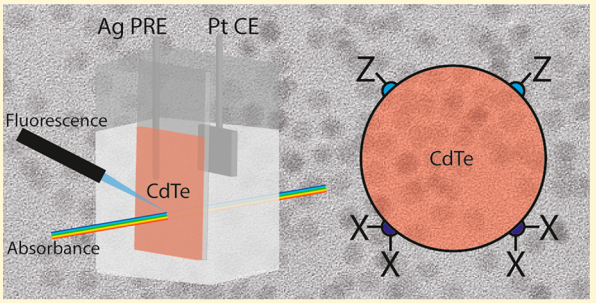

INTRODUCTION

The implementation of colloidal semiconductor nanocrystals (NCs) into optoelectronic devices is hindered by charge carrier trapping into states within the bandgap, which mainly arise due to dangling orbitals on the surface of these nanocrystals.[1−8] The passivation of these dangling orbitals has therefore been an extensive line of research.[2,5,8−12] Several strategies have been developed to understand and passivate these dangling orbitals, and hence, circumvent the nonradiative recombination pathways associated with them. For example, heteroepitaxial overgrowth of another semiconductor,[2,13] surface passivation with (in)organic ligands[10,14−17] and filling of trap states by Fermi level tuning[18] have all resulted in an increase in photoluminescence quantum yield (PLQY).[11,13,19] Interestingly, trap states are not necessarily detrimental as they can also be useful emissive centers,[20] temporarily store charge carriers for delayed luminescence,[21] or result in optical gain.[22] Therefore, improved understanding of the nature of these surface states will not only enable the rational design of passivation strategies for their removal, but may also offer new pathways to tailor the optoelectronic properties of colloidal nanomaterials.

Recently, DFT calculations have shown that the main contribution to in-gap states in Cd-chalcogenide NCs stems from undercoordinated surface chalcogen atoms (S, Se, Te).[9] Since the valence band (VB) maximum in CdTe NCs is formed predominantly by a linear combination of 5p Te orbitals, undercoordinated Te will result in trap states near the VB edge.[9] The conduction band (CB) is formed by the linear combination of the 5s Cd orbitals, which are less prone to trap state formation near the band edges due to their spherical symmetry.[9] However, the NC surface may be more complex and dynamic, which could give rise to Cd-related defect states.[17,23,24] For example, Cd−Cd dimers might form on the surface and the bonding orbital of these dimers could result in states within the bandgap, as has been suggested for Pb−Pb dimers in PbS NCs.[25] In principle, dangling orbitals on the surface can be passivated with (in)organic ligands, which are classified as L-, X-, and Z-type, depending on whether the ligands are two electron donors (L-type), one electron donors (X-type), or neutral two electron acceptors (Z-type).[10] Here,

Received: September 13, 2018
Revised: October 22, 2018
Published: October 23, 2018

DOI: 10.1021/acs.chemmater.8b03893
Chem. Mater. 2018, 30, 8052−8061

we use different trap state passivation strategies in combination with *in situ* spectroelectrochemistry and *ex situ* elemental analysis to elucidate the trap state distribution, the binding motifs of the passivating species and the effect of passivation of trap states in CdTe NC films.

Spectroelectrochemistry is a powerful tool to study important features of nanomaterials, such as the position of the band edges,[26−28] the degeneracy of the energy levels[29] and the distribution of trap states within the bandgap.[18,30,31] Since trapping of photogenerated charge carriers results in a decrease in PLQY, we use *in situ* photoluminescence spectroelectrochemistry to study the influence of the passivating ligands on the distribution of trap states. We correlate the observed spectroelectrochemical trends to the binding motifs of the passivating ligands with *ex situ* X-ray Photoelectron Spectroscopy (XPS) measurements, which suggests that X-type passivation leads to a 4-fold increase in PL intensity, whereas Z-type passivation results in almost a 40-fold increase in PL. Furthermore, after surface passivation the maximum number of injected electrons in the $1S_e$ level per nanocrystal increases, which suggests that competing surface redox reactions are slowed down. We hypothesize that X-type passivation with Cl^- occurs on Cd-related defect sites, such as Cd−Cd dimers, and Z-type passivation by $CdCl_2$ on undercoordinated Te sites. We show that undercoordinated Te surface sites contribute the most to the presence of in-gap states, since proper passivation with Z-type $CdCl_2$ ligands results in a drastic PL increase and a decrease of the PL dependence on the applied electrochemical potential. Our results shed light on the nature of surface binding sites in CdTe NCs and on how to passivate them with inorganic ligands.

EXPERIMENTAL SECTION

Materials. Oleic acid (OA, 90%), 1-octadecene (ODE, 90%), trioctylphosphine (TOP, 90%), 1,8-octanedithiol (8DT, ≥ 97%), cadmium chloride ($CdCl_2$, 99.99%), indium chloride ($InCl_3$, ≥ 99.999%), zinc chloride ($ZnCl_2$, 99.999%) and lithium perchlorate ($LiClO_4$, 99.99%) were purchased from Sigma-Aldrich. Cadmium oxide (CdO, 99.998%) and tellurium (Te, −18 + 60 mesh, 99.999%) were purchased from Alfa Aesar. The indium-doped tin oxide substrates (ITO, film thickness ∼100 nm, $R_{sq} \leq 20\ \Omega/cm^2$) were obtained from PGO Germany. Anhydrous acetone (≥99.8%) was purchased from VWR chemicals. Anhydrous methanol (MeOH, 99.8%), 1-butanol (BuOH, 99.8%), toluene (99.8%), and acetonitrile (99.99%) were all obtained from Sigma-Aldrich. Before use, the OA was degassed at 100 °C for 1 h, and the acetonitrile was dried by an Inert Technology PureSolv Micro Solvent Purification System. All other chemicals were used as-received. Cadmium and tellurium compounds are toxic and carcinogenic and should be handled with care.

Synthesis of CdTe NCs. The CdTe NCs were synthesized using the method of Kloper et al.[32] For the Cd-precursor, CdO (51.4 mg, 0.4 mmol) was mixed with OA (400 μL) and ODE (20 mL). The Te-precursor was prepared by dissolving elemental Te (51.0 mg, 0.4 mmol) in TOP (1 mL) and diluting the resulting yellow solution with ODE (4 mL). The Cd-precursor was first degassed under vacuum at 100 °C for approximately 1 h. Then, the system was flushed with N_2 and heated to ca. 280 °C until the red turbid mixture became a transparent colorless solution, indicating the formation of $Cd(OA)_2$. Subsequently, the temperature was raised to 310 °C for roughly 30 min. When the first gray precipitate of metallic Cd^0 was observed, the Te-precursor was swiftly injected. Following the resulting nucleation, the color of the solution quickly changed from yellow to black. The NCs were allowed to grow at 260 °C for 3 min, after which the mixture was quenched with 5 mL ODE. The Cd^0 was removed from the reaction mixture by centrifugation and decantation. Subsequent washing of the NCs was carried out by precipitating the NCs with a mixture of MeOH and BuOH (NCs:MeOH:BuOH 1:1:1), and centrifugation at 3500 rpm for ca. 3 min. The supernatant was decanted, and the NCs were resuspended in 5 mL toluene. This washing procedure was then repeated once more.

Nanocrystal Film Preparation. Nanocrystal films were prepared by dip-coating, using a Nima dipcoater. First, the ITO substrates were dipped for 30 s in a concentrated NC solution (∼10^{-4} M), followed by 30 s in a solution of 8DT in MeOH (0.1 M) and 30 s in MeOH to rinse off excess ligands. Using this procedure, 3−7 layers were applied to the ITO substrate. Roughly a third of the ITO was left uncoated to provide contact with the electrodes during the electrochemical measurements.

Treatment with Metal Chloride Salt Solutions. The NC films were passivated by treating them with either $CdCl_2$, $InCl_3$ or $ZnCl_2$ salt solutions in acetone. For that, the films were submersed overnight (∼16 h) in 2 mL of 0.1 M metal chloride salt in acetone solutions at room temperature. Due to the limited solubility of $CdCl_2$ in acetone, a saturated solution was used instead (estimated concentration <5 mM).[33] After the salt treatment, the films were rinsed with MeOH in order to remove unbound metal chloride salt.

Steady State Optical Spectroscopy. The absorbance of CdTe NC solutions and films was recorded on a PerkinElmer Lambda 900 UV/vis/NIR Spectrometer. The PL was measured on an Edinburgh Instruments FLS980 Fluorescence Spectrometer, using a 450 W xenon lamp as the excitation source. PLQY measurements were carried out in the same device, using an integrating sphere. Solutions were measured in closed quartz cuvettes (path length 10 mm). Diluted CdTe NC solutions were prepared by adding 50−100 μL of the crude NC in toluene solution (concentration ∼10^{-4} M) to 3 mL toluene in quartz cuvettes, in order to reach an optical density at the $1S_{3/2}1S_e$ transition between 0.1 and 0.5.

Spectroelectrochemistry. Spectroelectrochemical experiments were carried out in a glovebox under N_2. The setup consisted of a Ag wire pseudoreference electrode (PRE), a Pt sheet counter electrode (CE) and a CdTe-ITO film as working electrode (WE) in a quartz cell (Supporting Information, SI, Figure S1). The Ag wire (−4.90 ± 0.03 vs vacuum) was calibrated with ferrocene/ferrocenium (see SI Figure S2).[34] All potentials are given with respect to the Ag PRE. The supporting electrolyte consisted of a 0.1 M solution of $LiClO_4$ in acetonitrile. The potential was applied with an Autolab PGSTAT302N. Unless otherwise noted, a scan rate of 50 mV/s was used. Changes in absorbance were measured with a DH-2000 halogen lamp as light source, and detected with a USB2000 UV−vis spectrometer. All these components were acquired from Ocean Optics. For PL measurements, the films were excited with a 4.5 mW collimated laser diode from Thorlabs (wavelength 405 nm). The PL was detected with the same UV−vis spectrometer as used for the absorbance. For a schematic of the setup, see SI Figure S3.

Analysis of Band Edge Differential Absorption Signal. In order to separate the contributions to the spectroelectrochemical measurements arising from a bleach of the $1S_e$ transition and from a Stark shift, the signal was fitted with a sum of two components:

$$F_{Gauss}(\lambda) = A_{Gauss} \times e^{-(\lambda-\lambda_0)^2/(2\times\sigma^2)} \quad (1)$$

$$F_{Shift}(\lambda) = A_{Shift} \times \left(e^{-(\lambda-\lambda_0-\lambda_{Shift})^2/(2\times\sigma^2)} - e^{-(\lambda-\lambda_0)^2/(2\times\sigma^2)}\right) \quad (2)$$

where $F_{Gauss}(\lambda)$ is a Gaussian function describing the bleach due to state filling, and $F_{Shift}(\lambda)$ describes the Stark shift by a difference between two Gaussians, shifted from each other by λ_{Shift}. The fit is performed keeping λ_0 and σ fixed at the values determined by the fit of a single spectral slice, and letting A_{Gauss} and A_{Shift} vary. For λ_0 and σ this choice assumes that the distribution of energies for the bandgap of the NCs does not change along the scan. The value for λ_{Shift} is set to 17 nm, which allowed good agreement of the fitted function with the experimental data. In the SI we show that a small variation in the choice of λ_{Shift} does not affect the outcome of the fit. The value of A_{Gauss} is taken as the effective bleach of the $1S_e$ transition, while A_{Shift}

DOI: 10.1021/acs.chemmater.8b03893
Chem. Mater. 2018, 30, 8052−8061

is proportional to the amount of trapped charges per NC, as also shown in the SI.

Transmission Electron Microscopy (TEM) and Electron Diffraction. TEM samples were prepared by drop-casting a dilute solution of CdTe NCs in toluene on a carbon-coated copper TEM grid (400-mesh). TEM images and electron diffraction patterns were measured on a JEOL JEM-3200 FSC cryo-TEM, operating at 300 kV. The selected area electron diffraction (SAED) pattern was radially integrated to obtain the 1D electron diffraction pattern.[35]

X-ray Photoelectron Spectroscopy (XPS). XPS measurements were conducted on the CdTe-ITO WE described above, before and after the metal chloride salt treatments. Measurements were carried out on a Thermo Fisher K-Alpha spectrometer, using an Al K_α source (1486.7 eV). The C 1s peak at 284.8 eV was used as a reference to correct for shifts due to charging. While measuring, the pressure in the analysis chamber was kept below 2×10^{-7} mbar.

RESULTS AND DISCUSSION

CdTe NC Films. Spherical zinc blende CdTe NCs (native ligands: oleic acid) were obtained with a diameter of 6.0 ± 0.5 nm, as evidenced by Transmission Electron Microscopy (TEM, Figure 1a) and Electron Diffraction (ED, Figure 1b, c) measurements. Steady state optical measurements revealed sharp absorption features, with the $1S_{3/2}1S_e$ absorbance peak centered at 677 nm, and a narrow photoluminescence band centered at 690 nm (Figure 1d). The full-width-half-maximum (fwhm) was established to be 76 meV, and the photoluminescence quantum yield (PLQY) 9% (SI Figure S4). These CdTe NCs were dip-coated, with octanedithiol as cross-linking ligands, to form NC films (see Experimental Section), which led to a small red shift of the absorbance (to 679 nm) and PL peaks (to 691 nm, fwhm = 78 meV), as can be seen in Figure 1d.[36] The PLQY of the films is expected to drop below the value measured in solution due to energy-transfer.[37] These CdTe NC films are further characterized by *in situ* spectroelectrochemistry measurements, before and after treatment with metal chloride salt solutions, as will be described below.

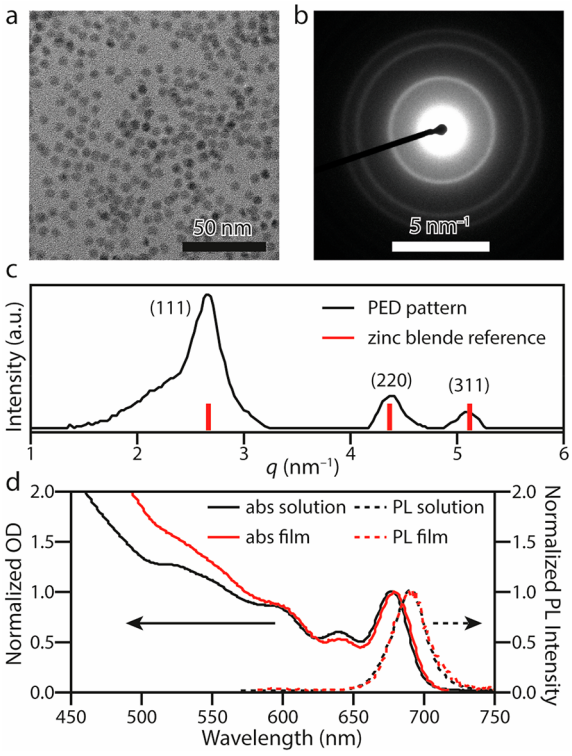

Figure 1. Structural and optical characterization of CdTe nanocrystals. (a) Transmission Electron Microscopy image, which reveals spherical nanocrystals (NCs) with a diameter of 6.0 ± 0.5 nm. (b) Electron Diffraction pattern of the NCs in panel a. (c) Azimuthal integration of the 2D ED pattern in panel b results in the 1D powder ED pattern, which reveals the zinc blende CdTe crystal structure. The red bars are from reference card 1010536 for zinc blende CdTe. (d) Steady-state UV−vis absorption (solid line) and PL spectra (dashed line) of CdTe NCs in solution (black lines) and in NC films, cross-linked with octanedithiol ligands (red lines).

Electrochemical Trap Filling in CdTe NC Films. The CdTe NC films were first analyzed with *in situ* absorbance and photoluminescence spectroelectrochemistry, prior to any passivation treatment (Figure 2). The potentials displayed are given with respect to a Ag pseudoreference electrode (PRE, −4.90 ± 0.03 V vs vacuum, calibrated with ferrocene/ferrocenium, see SI Figure S2). Cyclic voltammetry (scan rate 50 mV/s) was used to monitor the current and reversibility of the charge injection. The CV scan was started at −0.5 V (the open-circuit potential, V_{OC}). Upon scanning to more negative potentials, the negative current increases at an applied potential of −1.4 V, indicating the injection of electrons into the NC film (see SI Figure S5). When the scan direction is reversed, electrons are withdrawn from the NC film, indicated by the positive measured currents. We observe a clear offset between the first scan of the CV and the subsequent second and third scan (see SI Figure S5), which is indicative of trap state filling, as will be discussed in more detail below.

The differential absorbance as a function of applied potential is measured to quantify the charge injection into the CdTe NCs. Around an applied potential of −1.4 V, the $1S_{3/2}1S_e$ transition starts to be bleached (Figure 2a), which is indicative of charge injection into the bottom of the CB, and the bleach increases in intensity at more negative applied potentials until it reaches a maximum at an applied potential of −1.7 V vs Ag PRE (Figure 2b). Further, a sub-bandgap induced absorption feature around 700 nm is observed, which is attributed to a Stark shift,[38] i.e., a change in the energy of the NC absorption feature induced by the presence of neighboring charges. As a result, the $1S_{3/2}1S_e$ absorption peak is shifted to the red, resulting in more absorption at longer wavelengths, but less at the original location of the peak. This shift can be due to the presence of $1S_e$ electrons (a trion shift) or electrostatic interactions with localized surface charges. However, as can be seen in Figure 2a, b, the amplitude of the bleach is larger than that of the induced absorption, indicating that part of the bleach is also caused by state-filling of the $1S_e$ level.

We separate the Stark shift from the bleach due to state filling by a fit to the signal (see Experimental Sections), from which we deduce the effective bleach ΔA due to $1S_e$ level filling (Figure 2c, and SI Figure S6). ΔA is then converted to an average number of electrons in the $1S_e$ level per NC $< N_{1Se} >$ (left axis Figure 2c), by dividing it by the steady state absorbance (A_0), taking a degeneracy g of 2 electrons for the $1S_e$ level into account: $< N_{1Se} \geq g\Delta A/A_0$.[26,39−41] From this analysis it follows that at the most negative applied potential (−1.7 V vs Ag PRE) we inject on average 0.04 electrons/NC in the $1S_e$ level. This possibly indicates that many of the injected electrons get trapped or extracted by the reduction of impurities at the NC surface, and hence do not contribute to the $1S_{3/2}1S_e$ bleach. The presence of trapped electrons is also

DOI: 10.1021/acs.chemmater.8b03893
Chem. Mater. 2018, 30, 8052−8061

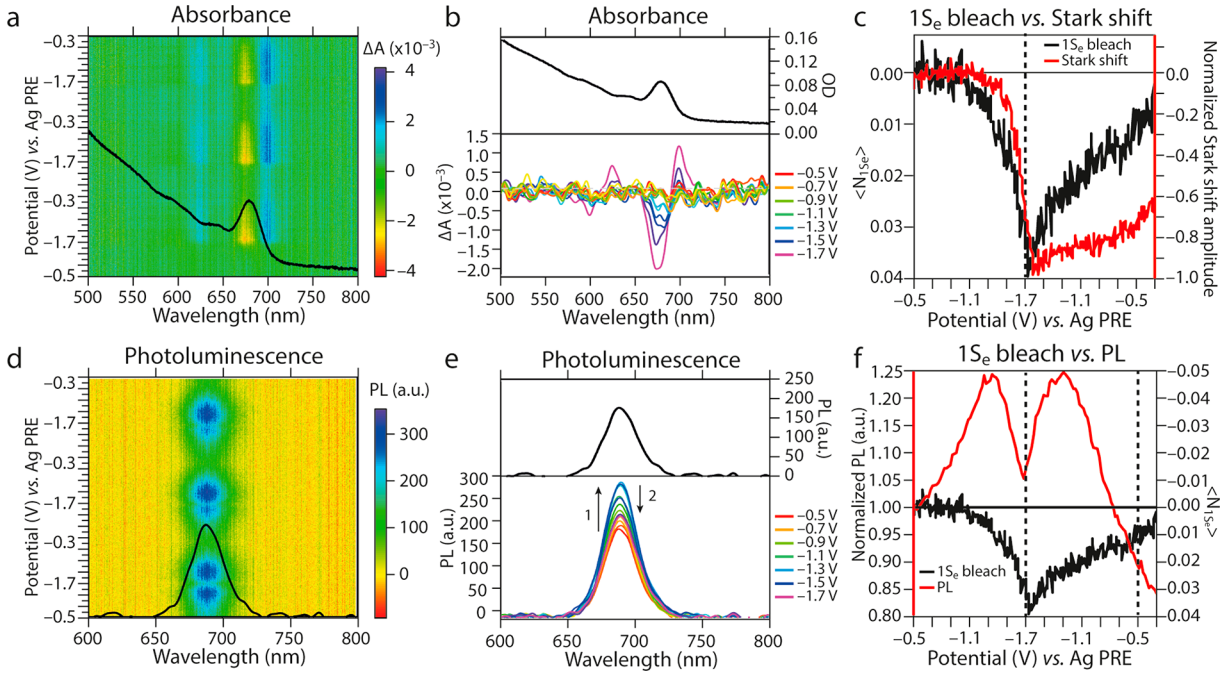

Figure 2. *In situ* spectroelectrochemistry on dithiol-capped CdTe NC films, prior to salt treatment. (a) 2D differential absorbance as a function of the applied potential for a bare CdTe NC Film. A bleach of the band edge transition is observed at applied potentials below −1.4 V, indicative of electron injection into the CB edge. (b) Smoothed spectral slices at different potentials of the absorbance spectra in (a). The steady state absorbance (A_0) is shown in black at the top. (c) Intensity of the band edge absorption bleach (at 677 nm) as a function of applied potential vs the Stark shift. On the left axis, the differential absorbance (ΔA) is divided by the steady state absorbance (A_0) and multiplied by the degeneracy of the CB edge ($g = 2$), which gives the average number of electrons (N_{1Se}) in the $1S_e$ level. The bleach was corrected for the Stark shift (red line, see also SI Figure S6). (d) 2D *In situ* PL spectra of the CdTe film as a function of applied potential. An increase in PL is clearly observed (potential range −0.5 to −1.3 V) before the PL band is quenched due to Auger recombination around −1.4 V. (e) Smoothed spectral slices of the PL spectra in (d). The PL first increases due to trap filling (arrow 1) and then decreases due to Auger recombination (arrow 2). The steady state PL spectrum at V_{oc} is shown in black at the top. (f) Intensity of the PL as a function of applied potential vs the bleach of the $1S_e$ level. The PL is very reversible and increases first due to trap filling (above −1.4 V), after which it decreases due to efficient Auger recombination (between −1.4 V and −1.7 V, dashed line). Above V_{oc} (applied potential > −0.5 V, dashed line), the PL decreases further due to an increase in electron trap states.

reflected in the hysteresis of the potential dependence of the $1S_{3/2}1S_e$ bleach and the Stark shift (Figure 2c), which shows that the NCs are still charged (giving rise to a Stark shift) whereas no electrons are in the $1S_e$ CB edge. We conclude that the Stark shift in absence of a band edge bleach is caused by electrons that occupy trap states within the bandgap, in line with earlier suggestions that traps can cause significant Stark shifts.[42,43]

Since the PLQY of CdTe NCs depends strongly on the electron occupation of trap states,[18] the *in situ* PL was measured as a function of the applied potential (Figure 2d) for the same CdTe NC film as described above. When the potential was scanned from −0.5 V (V_{oc}) to more negative potentials, charge injection into the CB can again be observed below −1.4 V (see CV in SI Figure S7). At these potentials a clear decrease of the PL is observed (Figure 2e), which we attribute to efficient Auger recombination of trions, as it coincides with the potential where the $1S_{3/2}1S_e$ absorption bleach initiates (Figure 3a, b). Interestingly, the PL first increases (up to an applied potential of −1.3 V, Figure 2d–f), before Auger recombination quenches it at lower potentials (lower than −1.4 V, Figure 2d–f). This PL increase is in line with our earlier observations[18] and is caused by filling of trap states as the Fermi level is raised, which reduces electron trapping and increases the PLQY (Figure 3a, b). The trapping rates of electrons ($\Gamma_{trap,e}$) and holes ($\Gamma_{trap,h}$) can be described as second order rate equations:

$$\Gamma_{trap,e} = k_{trap,e} N_{trap,empty} N_e \quad (3)$$

$$\Gamma_{trap,h} = k_{trap,h} N_{trap,full} N_h \quad (4)$$

The fact that trap filling leads to increased PL, shows that the electron capture rate constant $k_{trap,e}$ is much higher than the hole capture rate constant $k_{trap,h}$ in CdTe NCs (Figure 3a,b). We have previously argued that electron trapping is Auger assisted with the photogenerated hole being excited deeper into the valence band levels,[18] and others have seen similar effects for doped NCs[44] and core/shell heterostructures.[45]

We note that the change in PL is very reversible (Figure 2d, f). Furthermore, the PL drops below its initial value when a potential of −0.3 V is applied (i.e., a more positive potential than the V_{oc}), which can be assigned to an increase in the number of empty electron trap states, which decreases the PLQY because $\Gamma_{trap,e}$ increases. From this, the conclusion is drawn that the Fermi level in CdTe NC films at V_{oc} lies within a distribution of trap states (Figure 3a).

The results of the spectroelectrochemistry measurements were used to construct a model of the electron distribution in the system as a function of the Fermi-level position, depicted in Figure 3. From the hysteresis in potential dependence of the $1S_e$ bleach due to state filling and the Stark shift (Figure 2c), combined with the potential dependence of the PL intensity within the bandgap (Figure 2f), we argue that traps within the ensemble of CdTe NCs are quickly filled only when the Fermi level is above the $1S_e$ level. When the Fermi level is within the

DOI: 10.1021/acs.chemmater.8b03893
Chem. Mater. 2018, 30, 8052−8061

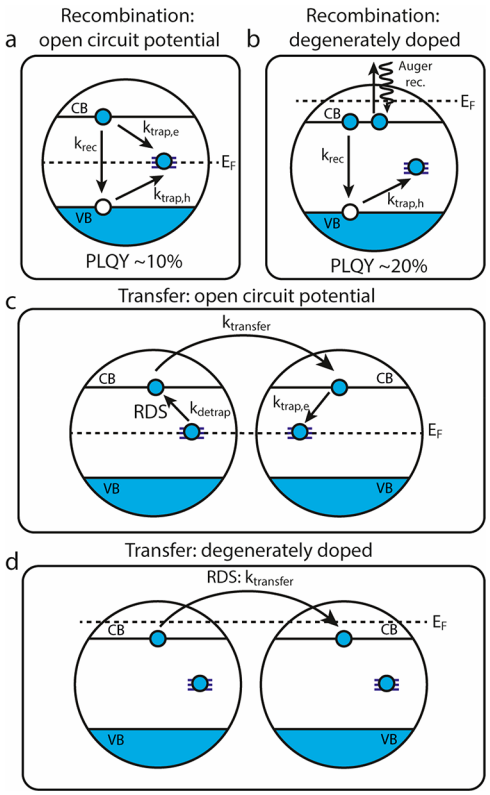

Figure 3. Charge carrier trapping, transfer and recombination in CdTe nanocrystals. (a) Recombination pathways in CdTe NCs. Photogenerated electrons and holes can recombine radiatively (k_{rec}), or charge carriers can get trapped (k_{trap}), which lowers the PLQY. (b) Recombination pathways in CdTe NCs with electrochemically filled trap states. Photogenerated electrons and holes can again recombine radiatively (k_{rec}), or charge carriers, in this case only holes, can get trapped ($k_{trap,h}$). Due to state filling of the CB edge, an additional nonradiative Auger recombination pathway opens up. (c) In unpassivated CdTe nanocrystals, in-gap states due to two coordinated Te (2c Te) and Cd-related defects are present at the NC surface. Charge carriers can transfer to a neighboring NC after thermally activated detrapping of trap states, followed by transfer via the band edges ($k_{transfer}$). The thermally activated detrapping is the rate-determining step (RDS). This detrapping slows down electron transfer by several orders of magnitude. The Fermi level (E_F) lies within the distribution of trap states (dashed line). (d) The in-gap states can be filled by raising the Fermi level (E_F, dashed line) above the CB edge, thereby enhancing the charge transfer between NCs and the PLQY.

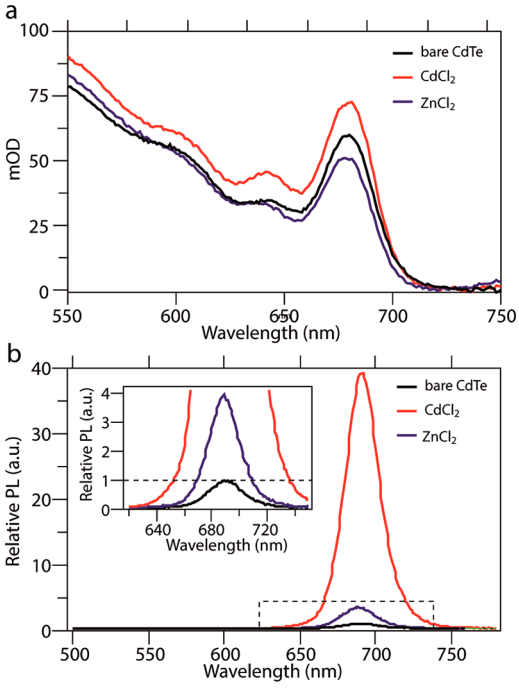

Figure 4. Influence of surface passivation on steady state absorbance and photoluminescence of CdTe films. (a) Absorbance and (b) photoluminescence (PL) spectra of thiol-capped CdTe NC films before and after treatment with $CdCl_2$ and $ZnCl_2$ in acetone solutions. The inset shows a zoom of the PL spectra of a bare CdTe NC film, and a film after $ZnCl_2$ treatment. The $1S_{3/2}1S_e$ absorbance does not shift after metal chloride salt treatment and a small variation in the intensity can be seen (panel a), but a much larger enhancement of the PL intensity after $ZnCl_2$ treatment (4-fold enhancement) and after $CdCl_2$ treatment (fourtyfold enhancement) were observed (panel b).

distribution of trap states, charge transfer between NCs has to be preceded by thermally activated detrapping to the CB (Figure 3c). This thermally activated detrapping (which is the rate-determining step, RDS) slows down electron transfer enormously by several orders of magnitude. If we assume an electron mobility of 10^{-2} $cm^2/(V\ s)$ for band edge electrons and thermally activated detrapping from a 0.5 eV deep trap state, then we can estimate that diffusion over the thickness d of a 100 nm thick NC film takes $t = \frac{d^2 k_B T}{e\mu \exp(-E_a / k_B T)} = 200$ s For band edge electrons (where the rate of injection is limited by cation diffusion with a diffusion coefficient of $\sim 10^{-7}$ cm^2/s)[28] charge injection over the entire film takes place on a ~1 ms time scale. So while electron injection/extraction from the conduction band may occur electrochemically reversibly, the filling/emptying of trap states is slow, resulting in the observed strong hysteresis.

This means that raising the Fermi level (E_F) above the trap states is not sufficient to fill all in-gap trap states within the NC film on a reasonable time scale, since the trap state transfer rate is very small and hence, only the first few layers of nanocrystals will have filled in-gap trap states (Figure 3c). This is also reflected in the fact that the Stark shift is negligible before the $1S_e$ CB edge is filled (only the first layer of NCs will have filled traps), but is present even though the band edge is emptied when the scan direction is reversed (Figure 2c). Only when E_F is raised above the CB edge (Figure 3d), charge carriers will quickly transfer between NCs due to reduced electron trapping in the first NC layer, and as a consequence, in-gap states throughout the entire NC film will be quickly filled due to electron injection, giving rise to a substantial Stark shift (Figure 2c). Raising the Fermi level above the $1S_e$ level also results in CB edge state filling, giving rise to additional nonradiative Auger recombination pathways (Figure 3b), which eventually competes with the other radiative and nonradiative processes discussed above.

Since the PLQY of bare CdTe NCs in solution is around 9% (SI Figure S4), a substantial part of the charge carriers recombine nonradiatively via in-gap trap states (Figure 3a), which therefore need to be efficiently removed. As mentioned above, these trap states can be filled electrochemically (Figure 3b, d) or passivated chemically, as we will discuss next.

Metal Chloride Salt Treatments and the Effect on the Steady State Optical Properties. We now have a toolset to

DOI: 10.1021/acs.chemmater.8b03893
Chem. Mater. 2018, 30, 8052−8061

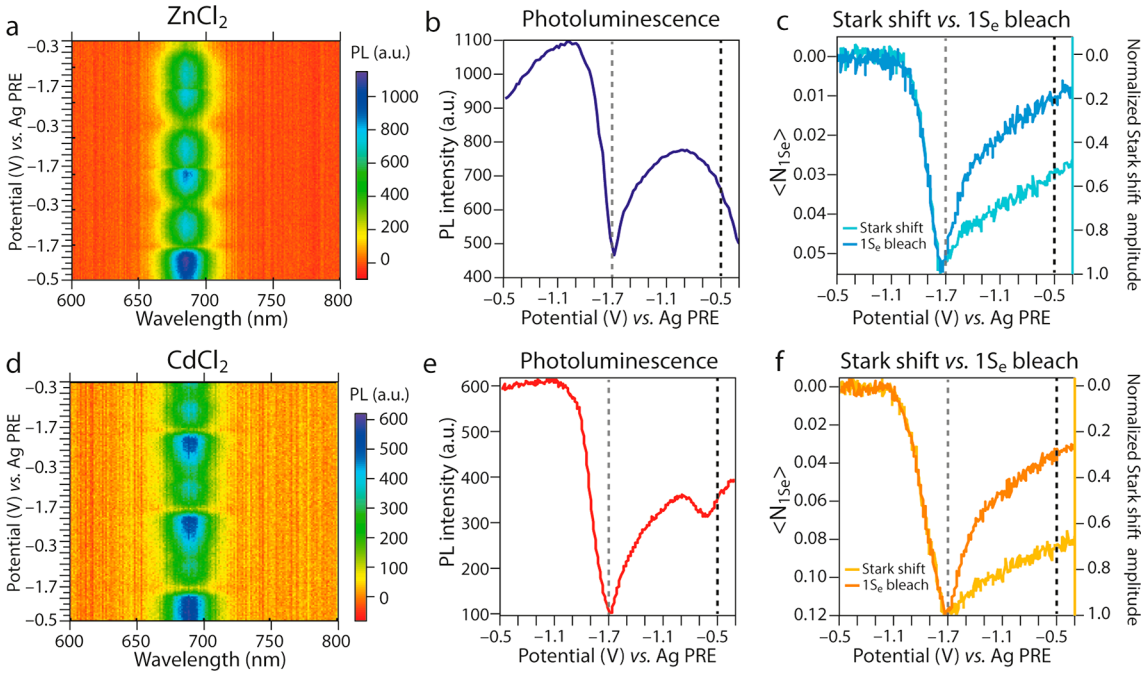

Figure 5. *In situ* photoluminescence (PL) spectroelectrochemistry on passivated CdTe NC films. (a) 2D *in situ* PL spectra as a function of applied potential for $ZnCl_2$ treated CdTe NC films. (b) Intensity of the PL peak (at 690 nm) as a function of applied potential of the spectra in (a) during the first cycle of the CV scan. (c) $\langle N_{1Se} \rangle$ (derived from the absorption bleach at 677 nm, blue line) as a function of applied potential for $ZnCl_2$ treated CdTe NC films. The average number of electrons in the band edge is ~0.05. The bleach is corrected for the Stark shift (light blue line, SI Figure S11). (d) 2D *in situ* PL spectra as a function of applied potential for $CdCl_2$ treated CdTe NC films. (e) Intensity of the PL peak (at 691 nm) as a function of applied potential of the spectra in (d) during the first cycle of the CV scan. (f) $\langle N_{1Se} \rangle$ (derived from the absorption bleach at 677 nm, orange line) as a function of applied potential for $CdCl_2$ treated CdTe NC films. The average number of electrons in the band edge is ~0.12. The bleach is corrected for the Stark shift (light orange line, SI Figure S12).

quantify the effect of trap states by *in situ* spectroelectrochemistry, which we will now discuss for CdTe NCs films that were passivated with various metal chloride salts. The CdTe NC films are placed in metal chloride salt solutions in acetone for ~16 h (see Experimental Section). This approach differs from previous work that reports solution phase surface passivation on CdTe NCs, since we are dealing with NC films that we do not want to detach from the substrate.[46]

First, we analyze the influence of trap state passivation with different metal chloride salt solutions on the optical properties of the CdTe nanocrystal films with steady state absorption and photoluminescence spectroscopy. As can be seen in Figure 4a, treatment with $CdCl_2$ and $ZnCl_2$ did not change the position and width of the band edge absorption. However, treatment with $InCl_3$ resulted in a shift of the band edge absorption to a lower wavelength, indicating that the NCs have decreased in size (SI Figure S8). Since $InCl_3$ is a strong Lewis acid, it is suggested that the blue-shift is due to etching of the NCs.[17,47] There is a dramatic increase in PL intensity (by a factor ~40) after $CdCl_2$ treatment (Figure 4b). This observation indicates that the PLQY of bare CdTe NCs in a dense NC film cannot exceed 2.5%, and that the PLQY has dropped compared to the value found for NCs in solution (9%, SI Figure S4), possibly due to energy transfer.[37] Treatment with $ZnCl_2$ also increases the PL intensity, but only by a factor ~4. Control experiments with acetone only showed small changes in PL intensity compared to the metal chloride salt in acetone solutions (SI Figure S8). As was also observed in the absorbance measurements, $InCl_3$ slightly blue-shifted the position of the PL band, possibly due to etching of the NCs, and the PL intensity has decreased slightly (SI Figure S9). These results show that treatment with $ZnCl_2$ and $CdCl_2$ salt solutions is effective in terms of PL enhancement, but the exact binding motif and the effect on the presence of in-gap trap states, remains unclear. Therefore, we perform the same *in situ* absorbance and PL spectroelectrochemistry measurements as discussed above for bare CdTe NC films after the metal chloride salt treatments.

In Situ Spectroelectrochemistry on Metal Chloride Treated CdTe Films. Figure 5 summarizes the *in situ* spectroelectrochemistry measurements after the CdTe NC films were treated with metal chloride salt solutions. The cyclic voltammograms show charge injection around −1.4 V, comparable to untreated CdTe NC films (SI Figure S10). As shown above, the PL of bare CdTe NC films depends heavily on the applied potential in the bandgap (Figure 2d–f), indicating the presence of in-gap trap states. Figure 5a–c shows that the PL of $ZnCl_2$ treated CdTe films depends only slightly on the applied potential (potential window −0.3 V until −1.4 V vs Ag PRE), although a minor increase in PL intensity is observed before efficient Auger recombination occurs around −1.4 V (vs Ag PRE). Differential absorbance measurements show that the charge injection is very reversible (Figure 5c). As before, the $1S_e$ bleach was corrected for the Stark shift (Figure 5c and SI Figure S11), which again shows hysteresis between the $1S_e$ bleach and the Stark shift, indicative of trap states.

The same *in situ* photoluminescence measurements on CdTe NC films treated with $CdCl_2$ in acetone solutions show that the PL of $CdCl_2$ treated CdTe NC films is nearly independent of the applied potential within the bandgap (potential window −0.3 V until −1.4 V vs Ag PRE, Figure 5d–

DOI: 10.1021/acs.chemmater.8b03893
Chem. Mater. 2018, 30, 8052−8061

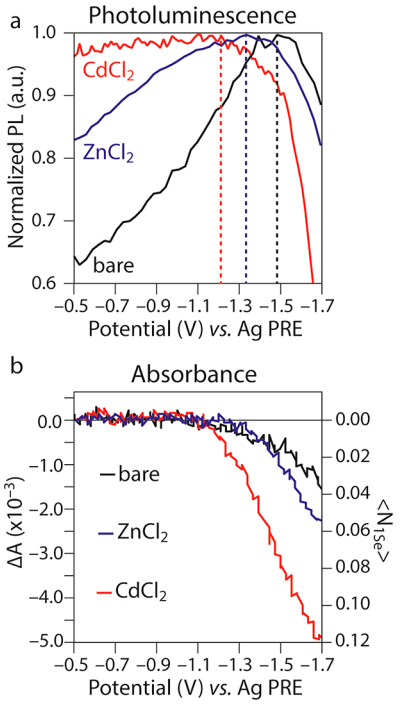

Figure 6. Comparison of *in situ* spectroelectrochemistry prior to and after metal chloride salt treatment. (a) Normalized PL intensity (at 691 nm) as a function of applied potential for CdTe NC films prior to (black line) and after metal chloride treatment (blue and red line). The PL drastically increases for untreated CdTe NCs before the band edge is reached when an electrochemical potential is applied (black line), whereas the PL is unaffected by the applied potential after $CdCl_2$ treatment (red line). The PL dependence of $ZnCl_2$ treated CdTe NC films lies in between. The onset of Auger recombination shifts to less negative potentials after treatment (indicated by the dashed lines). (b) Differential absorbance at the band edge (677 nm) as a function of applied potential for a bare CdTe NC film (black line) and CdTe NC films after $ZnCl_2$ (blue line) and $CdCl_2$ (red line) treatments. More electrons can be injected into the $1S_e$ level after metal chloride passivation, and the maximum bleach of the $1S_e$ level is not drastically shifted in potential by the treatments.

f). Furthermore, the PL is almost entirely quenched after charge injection into the CB, since all injected electrons contribute to nonradiative Auger recombination (Figure 5e). Again, differential absorbance measurements show that the charge injection is very reversible (Figure 5f). The $1S_e$ bleach was corrected for the Stark shift (Figure 5f and SI Figure S12), showing similar hysteresis between the $1S_e$ bleach and the Stark shift as observed above.

Figure 6a compares the dependence of the PL intensity on potential for the untreated film and the $ZnCl_2$ and $CdCl_2$ treated films. In all cases the PL decreases at very negative potentials due to Auger recombination with $1S_e$ electrons. However, the potential dependence in the bandgap due to trap filling is clearly reduced by the surface treatments. The PL increases by a factor of 1.28, 1.18, and 1.02 for bare CdTe films, $ZnCl_2$ treated films and $CdCl_2$ treated films, respectively, upon the application of a potential, right before the onset of efficient Auger recombination (around −1.4 V vs Ag PRE). The trend of the dependence of the PL intensity on the applied potential is in line with the increase in the steady state PL. Overall, $CdCl_2$ treatment results in a drastic enhancement of the PL intensity, and makes the PL less susceptible to the applied potential, suggesting that in-gap states have been effectively removed. These results imply that in-gap states are partially removed upon treatment with $ZnCl_2$ and almost completely removed by $CdCl_2$.

The variation of the PL intensity as a function of applied potential shows that the onset of Auger recombination shifts to less negative potentials after metal chloride treatment (dashed lines in Figure 6a). This could indicate that the surface treatment induced a shift of the band edges, as observed for several II−VI nanomaterials,[24] or that the onset of Auger recombination stays constant and the apparent shift is due to the suppression of electrochemical trap filling in the treated NCs. However, limits in the potential range that can be scanned without inducing sample degradation do not allow a proper spectroelectrochemical measurement of the CB position (Figure 6b).

When we compare the differential absorbance as a function of applied potential for the different CdTe NC films studied here, we find that more electrons per NC can be injected in the $1S_e$ level after metal chloride treatment under otherwise identical conditions (Figure 6b). The increase in the maximum number of $1S_e$ electrons correlates with the increase in PL

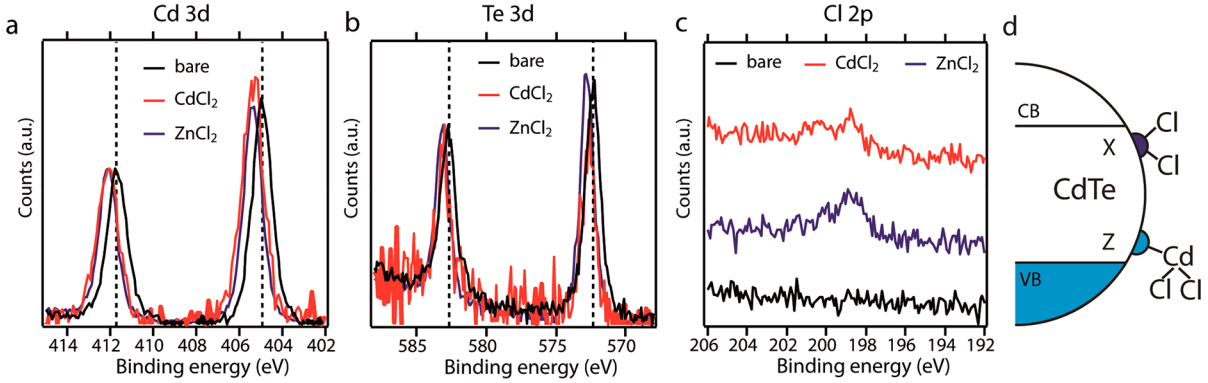

Figure 7. X-ray Photoelectron Spectroscopy (XPS) measurements. (a) Cd 3d, (b) Te 3d, and (c) Cl 2p XPS spectra of CdTe NC films prior to and after metal chloride treatment. The Cd and Te spectra have been normalized for the peak at a binding energy of around 412 and 583 eV, respectively. All films show the expected Cd and Te signals (slightly shifted with respect to the untreated film, panel a, b), and the metal chloride passivated films show a weak Cl peak ($ZnCl_2$, blue line, $CdCl_2$, red line), which was not present in the bare CdTe films (black line, panel c). (d) CdTe NCs contain Z- and X-type binding motifs on the surface, due to undercoordinated Te (light blue, Z-type passivation) and Cd-related defects (dark blue, X-type passivation), which therefore require different strategies for the complete passivation of the NC surface.

DOI: 10.1021/acs.chemmater.8b03893
Chem. Mater. 2018, 30, 8052−8061

Table 1. Quantification of the XPS Measurements

sample	cadmium (%)	tellurium (%)	chloride (%)	zinc/indium (%)	Cd:Te
bare CdTe	57	43			1.35
$CdCl_2$	59	28	12		2.10
$ZnCl_2$	54	37	9		1.45
$InCl_3$	42	42	10	6	0.99

intensity and the disappearance of the PL modulation with potential in the bandgap. We consider that the maximum number of $1S_e$ electrons depends on the rate that they are injected by the potentiostat as well as the rate that they disappear via reactions with, e.g., molecular oxygen or via surface electrochemical reactions. We think that such surface electrochemical reactions likely proceed via trap states, i.e., the first step of the electrochemical reduction of surface Cd^{2+} ions is the capturing of electrons in surface traps. This would suggest that passivating surface traps could reduce the rate at which $1S_e$ electrons disappear from the NCs and hence would increase the maximum steady state occupation of the $1S_e$ levels.

Elemental Analysis of the CdTe Nanocrystal Surface. Although the effect of the salt treatment is clearly observed by steady-state spectroscopy and *in situ* spectroelectrochemistry, the exact mechanism via which the NCs are passivated remains elusive. To investigate the nature of the passivation and the binding motif on the CdTe NC surface, X-ray Photoelectron Spectroscopy (XPS) was used. As can be seen in Figure 7 and Table 1, the bare CdTe NCs are cation rich with a Cd:Te ratio of 1.35. This is in agreement with the observation that NCs are often metal rich, where negative X-type ligands (e.g., carboxylates)[16] compensate for the excess positive charge of the metal cations.[10,17,24,48,49]

After treatment with $CdCl_2$ and $ZnCl_2$, small shifts of the Cd 3d and Te 3d spectra are observed (Figure 7a, b). Treatment of the NCs with $CdCl_2$ gives rise to a Cl signal which was not present for the bare CdTe NCs (Figure 7c). Additionally, the Cd:Te ratio increased to 2.10 (Table 1), indicating that more Cd is present with respect to bare CdTe NCs. These results suggest that the NCs are passivated via $CdCl_2$ Z-type ligands. We note that the Cd:Te ratio of 2.10 is too high for solely $CdCl_2$ passivated NC surfaces, which may indicate that some free $CdCl_2$ is present in the film. Treatment of the films with $ZnCl_2$ did not drastically alter the Cd:Te ratio (1.45 after treatment vs 1.35 prior to treatment). Interestingly, a clear Cl signal was observed for $ZnCl_2$ treated films, but no Zn was detected (SI Figure S13). This suggests that treatment with $ZnCl_2$ mainly results in X-type passivation by Cl^- ligands. Possibly, charge balance is ensured by other reactions at the surface, such as the loss of thiolate ligands. When NCs were treated with $InCl_3$, the Cd:Te ratio decreased to 0.99. This suggests that $InCl_3$ indeed etches the Cd-rich NCs, by stripping of $Cd(OA)_2$ Z-type ligands from the surface, as was suggested above. Furthermore, In is detected with XPS measurements, suggesting that $InCl_3$ or other In containing molecular species are adsorbed at the surface (SI Figure S14).

These results thus suggest a different type of surface passivation for the different chloride salts investigated here. Contrary to predictions that only undercoordinated Te surface atoms give rise to traps, which can be passivated with Z-type ligands,[9,46] these results suggest that X-type chloride ions can also passivate part of the traps present on the surface (Figure 7d). It seems likely that these chloride ions complex to surface Cd^{2+} ions and in doing so apparently passivate Cd localized trap states. While such traps were not found in recent DFT studies,[9] there could be more complicated Cd localized traps on the surface, not captured by these studies. For instance we can imagine that Cd−Cd dimers form dynamically on the surface and their bonding orbitals could act as traps, similar to suggestions of Pb−Pb dimer formation on the surface of PbS NCs.[25] Complexation of ligands (Cl^-, but perhaps also L-type ligands such as amines, which have also been shown to enhance the PL QY)[46] to surface Cd ions may prevent the formation of such Cd dimers (see also SI Discussion S1).

The different degree of passivation attained with the three metal chloride salts presented here may be partially explained by their solubility in acetone, which decreases as $ZnCl_2$ > $InCl_3$ > $CdCl_2$.[33] Since $ZnCl_2$ dissolves very well in acetone, it probably easily dissociates into Zn^{2+} and Cl^- ions, so that $ZnCl_2$ treatment will mainly passivate traps with X-type Cl^- ligands. $CdCl_2$, however, barely dissolves in acetone. As it forms complexes like $CdCl_4^{2-}$ in aqueous solutions, $CdCl_2$ in acetone may dissolve more like complexes or molecules than by dissociation into separate ions.[33] This may facilitate its binding as Z-type $CdCl_2$ to the NC, thus passivating the majority of the undercoordinated Te traps and hence increasing the PL.

CONCLUSIONS

We have studied the effect of metal chloride salt passivation on the presence of in-gap trap states in films of CdTe NCs by *in situ* absorbance and photoluminescence spectroelectrochemistry. Proper passivation of undercoordinated surface Te by Z-type ligands, like $CdCl_2$, results in a 40-fold increase in PL intensity. Additionally, surface passivation by these Z-type ligands makes the PL less dependent, or even independent, on the applied potential. Both observations show that the Z-type ligands efficiently passivate the majority of in-gap trap states in CdTe NCs. Treatment with $ZnCl_2$ in acetone results in a 4-fold increase in PL intensity, and an intermediate dependence of the PL intensity on the applied potential. Interestingly, we find no evidence of Zn on the CdTe NC films, whereas a clear Cl signal is observed with XPS. It is conjectured that chloride X-type passivation occurs at Cd-related sites at the surface. Our results show a spectroelectrochemical signature of two binding motifs on the surface of CdTe NCs, which can be properly passivated by a combination of X- and Z-type ligands.

ASSOCIATED CONTENT

Supporting Information

The Supporting Information is available free of charge on the ACS Publications website at DOI: 10.1021/acs.chemmater.8b03893.

A picture of the electrochemical cell, cyclic voltammograms of ferrocene/ferrocenium, schematic of the photoluminescence setup, photoluminescence quantum yield measurement, cyclic voltammograms prior to and after metal chloride salts treatments, Gaussian fits to Stark shifts, photoluminescence spectra before and after

DOI: 10.1021/acs.chemmater.8b03893
Chem. Mater. 2018, 30, 8052−8061

acetone solution treatment, absorption and photoluminescence spectra after $InCl_3$ treatment, XPS spectra Zn, XPS spectra In, and Supporting Discussion (PDF)

AUTHOR INFORMATION

Corresponding Authors

*E-mail: w.vanderstam@tudelft.nl.
*E-mail: a.j.houtepen@tudelft.nl.

ORCID

Ward van der Stam: 0000-0001-8155-5400
Nicholas Kirkwood: 0000-0002-7845-7081
Arjan J. Houtepen: 0000-0001-8328-443X

Author Contributions

§These authors contributed equally to this work.

Notes

The authors declare no competing financial interest.

ACKNOWLEDGMENTS

A.J.H. acknowledges support from the European Research Council Horizon 2020 ERC Grant Agreement No. 678004 (Doping on Demand). Bart Boshuizen is acknowledged for technical assistance during XPS measurements.

REFERENCES

(1) Kovalenko, M. V.; Manna, L.; Cabot, A.; Hens, Z.; Talapin, D. V.; Kagan, C. R.; Klimov, X. V. I.; Rogach, A. L.; Reiss, P.; Milliron, D. J.; Guyot-Sionnnest, P.; Konstantatos, G.; Parak, W. J.; Hyeon, T.; Korgel, B. A.; Murray, C. B.; Heiss, W. Prospects of Nanoscience with Nanocrystals. *ACS Nano* **2015**, *9*, 1012−1057.

(2) de Mello Donegá, C. Synthesis and Properties of Colloidal Heteronanocrystals. *Chem. Soc. Rev.* **2011**, *40*, 1512−1546.

(3) Reiss, P.; Protière, M.; Li, L. Core/Shell Semiconductor Nanocrystals. *Small* **2009**, *5*, 154−168.

(4) Burda, C.; Chen, X.; Narayanan, R.; El-Sayed, M. A. Chemistry and Properties of Nanocrystals of Different Shapes. *Chem. Rev.* **2005**, *105*, 1025−1102.

(5) Kagan, C. R.; Murray, C. B. Charge Transport in Strongly Coupled Quantum Dot Solids. *Nat. Nanotechnol.* **2015**, *10*, 1013−1026.

(6) Talapin, D. V.; Lee, J. S.; Kovalenko, M. V.; Shevchenko, E. V. Prospects of Colloidal Nanocrystals for Electronic and Optoelectronic Applications. *Chem. Rev.* **2010**, *110*, 389−458.

(7) Kim, J.; Kotov, N. A. Charge Transport Dilemma of Solution-Processed Nanomaterials. *Chem. Mater.* **2014**, *26*, 134−152.

(8) Wuister, S.; de Mello Donega, C.; Meijerink, A. Influence of Thiol Capping on the Exciton Luminescence and Decay Kinetics of CdTe and CdSe Quantum Dots. *J. Phys. Chem. B* **2004**, *108*, 17393−17397.

(9) Houtepen, A. J.; Hens, Z.; Owen, J. S.; Infante, I. On the Origin of Surface Traps in Colloidal II-VI Semiconductor Nanocrystals. *Chem. Mater.* **2017**, *29*, 752−761.

(10) Anderson, N. C.; Hendricks, M. P.; Choi, J. J.; Owen, J. S. Ligand Exchange and the Stoichiometry of Metal Chalcogenide Nanocrystals: Spectroscopic Observation of Facile Metal-Carboxylate Displacement and Binding. *J. Am. Chem. Soc.* **2013**, *135*, 18536−18548.

(11) Pu, C.; Peng, X. To Battle Surface Traps on CdSe/CdS Core/Shell Nanocrystals: Shell Isolation versus Surface Treatment. *J. Am. Chem. Soc.* **2016**, *138*, 8134−8142.

(12) Giansante, C.; Infante, I. Surface Traps in Colloidal Quantum Dots: A Combined Experimental and Theoretical Perspective. *J. Phys. Chem. Lett.* **2017**, *8*, 5209−5215.

(13) Boldt, K.; Kirkwood, N.; Beane, G. A.; Mulvaney, P. Synthesis of Highly Luminescent and Photo-Stable, Graded Shell CdSe/$Cd_xZn_{1-x}S$ Nanoparticles by *In Situ* Alloying. *Chem. Mater.* **2013**, *25*, 4731−4738.

(14) Chen, P. E.; Anderson, N. C.; Norman, Z. M.; Owen, J. S. Tight Binding of Carboxylate, Phosphonate, and Carbamate Anions to Stoichiometric CdSe Nanocrystals. *J. Am. Chem. Soc.* **2017**, *139*, 3227−3236.

(15) Drijvers, E.; de Roo, J.; Martins, J. C.; Infante, I.; Hens, Z. Ligand Displacement Exposes Binding Site Heterogeneity on CdSe Nanocrystal Surfaces. *Chem. Mater.* **2018**, *30*, 1178−1186.

(16) De Nolf, K.; Cosseddu, S. M.; Jasieniak, J. J.; Drijvers, E.; Martins, J. C.; Infante, I.; Hens, Z. Binding and Packing in Two-Component Colloidal Quantum Dot Ligand Shells: Linear versus Branched Carboxylates. *J. Am. Chem. Soc.* **2017**, *139*, 3456−3464.

(17) Greaney, M. J.; Couderc, E.; Zhao, J.; Nail, B. A.; Mecklenburg, M.; Thornbury, W.; Osterloh, F. E.; Bradforth, S. E.; Brutchey, R. L. Controlling the Trap State Landscape of Colloidal CdSe Nanocrystals with Cadmium Halide Ligands. *Chem. Mater.* **2015**, *27*, 744−756.

(18) Boehme, S. C.; Azpiroz, J. M.; Aulin, Y. V.; Grozema, F. C.; Vanmaekelbergh, D.; Siebbeles, L. D. A.; Infante, I.; Houtepen, A. J. Density of Trap States and Auger-Mediated Electron Trapping in CdTe Quantum-Dot Solids. *Nano Lett.* **2015**, *15*, 3056−3066.

(19) Zhou, J.; Zhu, M.; Meng, R.; Qin, H.; Peng, X. Ideal CdSe/CdS Core/Shell Nanocrystals Enabled by Entropic Ligands and Their Core Size-, Shell Thickness-, and Ligand-Dependent Photoluminescence Properties. *J. Am. Chem. Soc.* **2017**, *139*, 16556−16567.

(20) Berends, A. C.; Rabouw, F. T.; Spoor, F. C. M.; Bladt, E.; Grozema, F. C.; Houtepen, A. J.; Siebbeles, L. D. A.; De Mello Donega, C. Radiative and Nonradiative Recombination in $CuInS_2$ Nanocrystals and $CuInS_2$-Based Core/Shell Nanocrystals. *J. Phys. Chem. Lett.* **2016**, *7*, 3503−3509.

(21) Rabouw, F. T.; Kamp, M.; van Dijk-Moes, R. J. A.; Gamelin, D. R.; Koenderink, A. F.; Meijerink, A.; Vanmaekelbergh, D. Delayed Exciton Emission and Its Relation to Blinking in CdSe Quantum Dots. *Nano Lett.* **2015**, *15*, 7718−7725.

(22) Geiregat, P.; Houtepen, A. J.; Sagar, L. K.; Infante, I.; Zapata, F.; Grigel, V.; Allan, G.; Delerue, C.; Van Thourhout, D.; Hens, Z. Continuous-Wave Infrared Optical Gain and Amplified Spontaneous Emission at Ultralow Threshold by Colloidal HgTe Quantum Dots. *Nat. Mater.* **2017**, *17*, 35−42.

(23) Buckley, J. J.; Couderc, E.; Greaney, M. J.; Munteanu, J.; Riche, C. T.; Bradforth, S. E.; Brutchey, R. L. Chalcogenol Ligand Toolbox for CdSe Nanocrystals and Their Influence on Exciton Relaxation Pathways. *ACS Nano* **2014**, *8*, 2512−2521.

(24) Boles, M. A.; Ling, D.; Hyeon, T.; Talapin, D. V. The Surface Science of Nanocrystals. *Nat. Mater.* **2016**, *15*, 141−154.

(25) Voznyy, O.; Thon, S. M.; Ip, A. H.; Sargent, E. H. Dynamic Trap Formation and Elimination in Colloidal Quantum Dots. *J. Phys. Chem. Lett.* **2013**, *4*, 987−992.

(26) Boehme, S. C.; Vanmaekelbergh, D.; Evers, W. H.; Siebbeles, L. D. A.; Houtepen, A. J. In Situ Spectroelectrochemical Determination of Energy Levels and Energy Level Offsets in Quantum-Dot Heterojunctions. *J. Phys. Chem. C* **2016**, *120*, 5164−5173.

(27) Chen, M.; Guyot-Sionnest, P. Reversible Electrochemistry of Mercury Chalcogenide Colloidal Quantum Dot Films. *ACS Nano* **2017**, *11*, 4165−4173.

(28) Gudjonsdottir, S.; van der Stam, W.; Kirkwood, N.; Evers, W. H.; Houtepen, A. J. The Role of Dopant Ions on Charge Injection and Transport in Electrochemically Doped Quantum Dot Films. *J. Am. Chem. Soc.* **2018**, *140*, 6582−6590.

(29) Wehrenberg, B. L.; Yu, D.; Ma, J.; Guyot-Sionnest, P. Conduction in Charged PbSe Nanocrystal Films. *J. Phys. Chem. B* **2005**, *109*, 20192−20199.

(30) van der Stam, W.; Gudjonsdottir, S.; Evers, W. H.; Houtepen, A. J. Switching between Plasmonic and Fluorescent Copper Sulfide Nanocrystals. *J. Am. Chem. Soc.* **2017**, *139*, 13208−13217.

(31) Pinchetti, V.; Lorenzon, M.; Mcdaniel, H.; Meinardi, F.; Klimov, V. I.; Brovelli, S.; Lorenzi, R. Spectro-Electrochemical Probing of Intrinsic and Extrinsic Processes in Exciton Recombination in I-III-VI_2 Nanocrystals. *Nano Lett.* **2017**, *17*, 4508−4517.

DOI: 10.1021/acs.chemmater.8b03893
Chem. Mater. 2018, 30, 8052−8061

(32) Kloper, V.; Osovsky, R.; Kolny-Olesiak, J.; Sashchiuk, A.; Lifshitz, E. The Growth of Colloidal Cadmium Telluride Nanocrystal Quantum Dots in the Presence of Cd^0 Nanoparticles. *J. Phys. Chem. C* **2007**, *111*, 10336−10341.
(33) Vanderzee, C. E.; Dawson, H. J. The Stability Constants of Cadmium Chloride Complexes: Variation with Temperature and Ionic Strength. *J. Am. Chem. Soc.* **1953**, *75*, 5659−5663.
(34) Ruch, P. W.; Cericola, D.; Hahn, M.; Kötz, R.; Wokaun, A. On the Use of Activated Carbon as a Quasi-Reference Electrode in Non-Aqueous Electrolyte Solutions. *J. Electroanal. Chem.* **2009**, *636*, 128−131.
(35) Klinger, M.; Jager, A. Computer Programs Crystallographic Tool Box (CrysTBox): Automated Tools for Transmission Electron Microscopists and Crystallographers. *J. Appl. Crystallogr.* **2015**, *48*, 2012−2018.
(36) Klimov, V. I.; Ivanov, S. A.; Nanda, J.; Achermann, M.; Bezel, I.; McGuire, J. A.; Piryatinski, A. Single-Exciton Optical Gain in Semiconductor Nanocrystals. *Nature* **2007**, *447*, 441−446.
(37) Rogach, A. L.; Klar, T. A.; Lupton, J. M.; Meijerink, A.; Feldmann, J. Energy Transfer with Semiconductor Nanocrystals. *J. Mater. Chem.* **2009**, *19*, 1208−1221.
(38) Klimov, V. I. Optical Nonlinearities and Ultrafast Carrier Dynamics in Semiconductor Nanocrystals. *J. Phys. Chem. B* **2000**, *104*, 6112−6123.
(39) Puntambekar, A.; Wang, Q.; Miller, L.; Smieszek, N.; Chakrapani, V. Electrochemical Charging of CdSe Quantum Dots: Effects of Adsorption *Versus* Intercalation. *ACS Nano* **2016**, *10*, 10988−10999.
(40) Brozek, C. K.; Hartstein, K. H.; Gamelin, D. R. Potentiometric Titrations for Measuring the Capacitance of Colloidal Photodoped ZnO Nanocrystals. *J. Am. Chem. Soc.* **2016**, *138*, 10605−10610.
(41) Carroll, G. M.; Tsui, E. Y.; Brozek, C. K.; Gamelin, D. R. Spectroelectrochemical Measurement of Surface Electrostatic Contributions to Colloidal CdSe Nanocrystal Redox Potentials. *Chem. Mater.* **2016**, *28*, 7912−7918.
(42) Houtepen, A. J.; Vanmaekelbergh, D. Orbital Occupation in Electron-Charged CdSe Quantum-Dot Solids. *J. Phys. Chem. B* **2005**, *109*, 19634−19642.
(43) Grimaldi, G.; Crisp, R. W.; ten Brinck, S.; Zapata, F.; van Ouwendorp, M.; Renaud, N.; Kirkwood, N.; Evers, W. H.; Kinge, S.; Infante, I.; Siebbeles, L. D. A.; Houtepen, A. J. Hot-Electron Transfer in Quantum-Dot Heterojunction Films. *Nat. Commun.* **2018**, *9*, 2310−2319.
(44) Brovelli, S.; Galland, C.; Viswanatha, R.; Klimov, V. I. Tuning Radiative Recombination in Cu-Doped Nanocrystals *via* Electrochemical Control of Surface Trapping. *Nano Lett.* **2012**, *12*, 4372−4379.
(45) Brovelli, S.; Bae, W. K.; Meinardi, F.; González, B. S.; Lorenzon, M.; Galland, C.; Klimov, V. I. Electrochemical Control of Two-Color Emission from Colloidal Dot-in-Bulk Nanocrystals. *Nano Lett.* **2014**, *14*, 3855−3863.
(46) Kirkwood, N.; Monchen, J. O. V.; Crisp, R. W.; Grimaldi, G.; Bergstein, H.; du Fossé, I.; van der Stam, W.; Infante, I.; Houtepen, A. J. Finding and Fixing Traps in II-VI and III-V Colloidal Quantum Dots: The Importance of Z-type Ligand Passivation. *J. Am. Chem. Soc.* **2018**, DOI: 10.1021/ja-2018-07783h.
(47) Pearson, R. Absolute Electronegativity and Hardness: Application to Inorganic Chemistry. *Inorg. Chem.* **1988**, *8441*, 3533−3539.
(48) Luther, J. M.; Pietryga, J. M. Stoichiometry Control in Quantum Dots : A Viable Analog to Impurity Doping of Bulk Materials. *ACS Nano* **2013**, *7*, 1845−1849.
(49) Protesescu, L.; Nachtegaal, M.; Voznyy, O.; Borovinskaya, O.; Rossini, A. J.; Emsley, L.; Copéret, C.; Günther, D.; Sargent, E. H.; Kovalenko, M. V. Atomistic Description of Thiostannate-Capped CdSe Nanocrystals: Retention of Four-Coordinate SnS_4 Motif and Preservation of Cd-Rich Stoichiometry. *J. Am. Chem. Soc.* **2015**, *137*, 1862−1874.

DOI: 10.1021/acs.chemmater.8b03893
Chem. Mater. 2018, 30, 8052−8061